Microwave assisted freezing
Part 1: Experimental investigation and numerical modeling

Mathieu SADOT, Sébastien CURET, Alain LE-BAIL, Olivier ROUAUD, Michel HAVET

Abstract

The aim of this study was to develop an innovative process dedicated to enhancing the quality of frozen food using microwaves. A microwave assisted freezing device was designed at the laboratory scale to perform experiments in controlled conditions. Small samples of methylcellulose gels were frozen using nitrogen gas in a TE_{10} waveguide, where microwaves at 2.45 GHz were emitted intermittently or continuously. A numerical model was also developed to obtain results difficult to measure such as the local electric field and the corresponding energy density. The phase change part of the model was based on an enthalpy formulation and on the growth of spherical ice crystals. An original “hybrid 2D-3D” solving methodology was used to reduce the duration of the simulations. Favourable comparisons between the predicted temperatures and the experimental data highlighted the relevance of the models used for the thermophysical and dielectric properties. The analysis of the interactions between microwaves and matter, performed with numerical simulations, revealed the role of the freezing front as a boundary. The strong influence of sample size and of dielectric properties on the power density distribution were also illustrated when comparing our results with those published previously. The scientific knowledge obtained through this study and the original structure of the numerical model will be used to optimize microwave assisted freezing and link the process parameters to the reduction of ice crystal size highlighted in the companion paper.

Keywords

Freezing; microwaves; modelling; ice fraction;

Highlights

- A device was built to perform microwave assisted freezing in a controlled configuration.
- A hybrid 2D-3D model was developed to decrease computation time.
- The numerical model was validated against experimental results.
- All food properties were modelled using the ice fraction during freezing.
- The interactions between the EM field and the freezing front were highlighted by the simulations.

Industrial relevance

Microwave assistance during freezing can improve frozen product quality by reducing ice crystal size. This innovative and promising process has not yet been given much attention. Developing an accurate model which describes microwave – matter interactions during phase change permits numerical simulations that can facilitate the design of industrial equipment, and determine optimal product dimensions.

1. Introduction

Freezing is one of the most widely used conservation processes in the food industry; low storage temperatures allow good preservation of product organoleptic (texture, taste, appearance) and nutritive (vitamins, minerals) qualities. It reduces chemical reaction rates (Lim et al., 2004) and controls microbial activity (Bremer & Ridley, 2004).

The quality of a frozen product is generally better when smaller ice crystals are formed (Delgado & Sun, 2001) because larger ones damage cell membranes due to water expansion during the phase change (Kalichevsky et al., 1995). These small crystals are usually obtained for faster freezing processes (Devine et al., 1996) but fast freezing processes (e.g. cryogenics) are known to be energy-demanding (Chourot et al., 2003; Dempsey & Bansal, 2012).

In recent years, growing interest in innovative freezing processes has led to increased frozen product quality while reducing ice crystal size, using ultrasound, magnetic fields, AC and DC electric fields, mechanical agitation, and pressure shift freezing (Dalvi-Isfahan et al., 2017; Jha et al., 2017; Le Bail et al., 2002; Woo & Mujumdar, 2010). Electromagnetic wave assisted freezing is one of the less investigated processes although some studies have presented interesting results. Apart from the simple main principle that consists in applying an electromagnetic field during the freezing process, it entails several modalities and configurations. It was first studied by Hanyu et al. (1992) and Jackson et al.(1997) who used 2450 MHz microwave irradiation on non-food material during freezing. Hanyu et al.(1992) found a reduction in ice crystal size in squid retina that resulted in better ultrastructural preservation. Jackson et al. (1997) obtained less ice and more glass in an aqueous ethylene glycol solution. More recent works have focused on electromagnetic wave assistance during food freezing. Anese et al. (2012) and Hafezparast-moadab et al. (2018) used 27.12 MHz radiofrequency (RF) wave irradiation during freezing. Anese et al. (2012) froze pork with liquid nitrogen and obtained better product quality when the product was frozen under electromagnetic wave irradiation. The crystals were also found to be smaller with the use of RF assistance. Hafezparast-moadab et al. (2018) froze

trout with a cold air convection system with and without RF assistance. They observed a reduction in ice crystal size up to 75% in the better case in comparison to conventional freezing. Microwave assisted freezing at 2450 MHz was investigated by Xanthakis et al. (2014). They also showed a reduction in ice crystal size when microwave assistance was used.

Despite these promising results, there is a lack of information on the physical mechanisms involved in the improvement of the freezing process by microwaves. The European FREEZEWAVE project (FP7-ERA-Net SUSFOOD) was initiated to help understanding these phenomena. The project goals were to develop and optimize a lab scale batch process and to develop a new model in order to improve scientific knowledge on microwave assisted process. This project also aimed to assess the effect of microwaves on reduction of the ice crystal size to improve frozen foods quality and scale up to industrial scale for batch and continuous processes.

Most of the experiments anterior to FREEZEWAVE project were performed in multi-mode cavities where microwave distribution is heterogeneous and cannot be determined; especially in the case of pulsed or intermittent waves. In the duty cycles applied temperature fluctuations were considered to be at the origin of promising results, but interactions between the matrices and the microwaves could not be analysed in-depth. The only numerical study on the interaction of microwaves and matter during freezing was performed previously in the FREEZEWAVE project to help obtain better understanding of these phenomena (Sadot et al., 2017). The resonance phenomena inside the product were identified and revealed the displacement of hot spots during the phase change, induced by the decrease in dielectric properties with temperature. Nevertheless, this pioneering work was based on a model that was not validated against the experimental data of a microwave assisted freezing process. Moreover, the physical and electrical properties were taken from the literature.

Taking into account these considerations, the aim of the current study is to: (i) design an experimental device to conduct microwave assisted freezing experiments in controlled conditions with temperature measurements inside the matrices; (ii) conduct experiments on a small sample in which the treatment is expected to be homogeneous; (iii) define and use protocols in order to measure the properties required as inputs in the model; and (iv) validate the model against real experimental data.

2. Materials and methods

2.1. Product

For this study, experiments had to be conducted on a homogeneous product, which can be made with good repeatability, in order to conserve the same properties. This is why we chose methylcellulose gel whose thermophysical and dielectric properties are close to those of food,

especially meat (Pangrle et al., 1992; Taoukis et al., 1987; Zhang & Datta, 2005). Methylcellulose gels at 13% (w/w) were prepared by progressively adding 15 g of methylcellulose powder (Tylose H 100000 YP2, ShinEtsu, Jp) into 100 g of demineralized water agitated with a magnetic stirrer. The solution was then poured into a Polyether ether ketone (PEEK) mould of 10 mm height, 39 mm length and 9 mm width and hermetically stored at 4°C for at least 10 h. To avoid the development of microorganisms and the occurrence of air bubbles, the gel was not stored for more than 4 days. The PEEK moulds were inserted into polystyrene sample holders to ensure good insulation during the freezing experiments.

2.2. Experimental device

An experimental device was developed (Figure 1) to study the microwave assisted freezing of this gel in controlled conditions. In the FREEZEWAVE project, this device must also be able to treat real food matrices.

Nitrogen is transferred from a compressed gas cylinder (1) into a liquid nitrogen tank (2), in which a steel pipe is immerged. The liquid nitrogen is injected into the pipe where it vaporises and increases in temperature. The end of the pipe is equipped with a heating part (3) used to control the temperature at the inlet of the applicator (4) in which the product (5) is placed. The applicator is located in a rectangular waveguide WR 340 (section 86 mm x 43 mm), to ensure the propagation of the fundamental single-mode TE_{10} at a frequency of 2450 MHz (electric field perpendicular to the wave propagation direction with an extremum at the centre of the long walls, a zero value at the small walls and a constant value along the small side). Two slits of 10 mm height, perpendicular to the microwave propagation direction, were machined along the small walls of the applicator flange to allow the inlet and the outlet of the nitrogen gas. The nitrogen gas is then extracted outside the building in which the experiment takes place. Holes of 0.5 mm were drilled every 5 mm along the centre of the small waveguide wall to insert sheathed thermocouples through the waveguide, the polystyrene and the PEEK to the sample in order to measure temperature during microwave assisted freezing. Thermocouples, electrically connected to the waveguide walls, are sheathed/isolated to avoid electric arc formation.

Microwaves are continuously emitted by a solid-state generator (GMS200, SAIREM, France) (6). They are transmitted to the waveguide via a switch (7). This permits the generation of pulses by sending the microwaves alternatively to an adapted absorptive load (8) and to an antenna (9) located at the inlet of the waveguide. After passing through the microwave applicator, the microwave power transmitted is absorbed by a water-load (10) to avoid any reflection.

With this configuration, microwaves and nitrogen reach the product on the top surface. The microwaves are expected to pass through the frozen product with very little attenuation because of the low dielectric properties of the frozen product. Therefore, the microwaves can act on the phase change via the hot spots able to follow the freezing front (Sadot et al., 2017). Unlike this previous numerical study, the product does not fill the entire waveguide cross-section. The mould containing the sample is centred as shown in Figure 1 (11) and surrounded by polystyrene (except the cooled surface) to ensure thermal insulation. The sheathed thermocouples are inserted at depths of 2 mm and 7 mm (along the z axis), as shown in Figure 2.

3. Model

The model used in this study is based on an enthalpy formulation of the heat equation (Eq. 1) with a source term derived from Maxwell equation (Eq. 2).

$$\frac{\partial H}{\partial t}\rho - \nabla . k\nabla T = Q \quad (1)$$

$$Q = \frac{1}{2}\omega\varepsilon_0\varepsilon''|E_{local}|^2 \quad (2)$$

This model was developed previously and is fully detailed in Sadot et al. (2017). The phase change model is based on the ice mass fraction that depends on crystal volume growth. The thermophysical and dielectric properties vary with the ice mass fraction as the water state is assumed to be the only parameter responsible for the variation of properties.

3.1. Hypotheses and boundary conditions

Several hypotheses are made to model the system:

_The product is assumed to be homogeneous.

_The mass transfer is neglected because of the small specific area and the speed of cryogenic freezing (Delgado & Sun, 2001; Hallstrom, 1990).

Heat transfer equations are solved only in the product sample with the following boundaries:

_The initial temperature is assumed constant within the product.

$T = T_0$ at $t = 0, \forall\ x, y, z$ (3)

_The heat transfer between the product and the nitrogen is assumed to be homogeneous on the entire surface.

$n(k\nabla T) = -h(T-T_{N2})$ at $z = 0$ (top surface), $\forall\ x, y$ (4)

_The lateral walls of the product exchange heat with a global transfer loss coefficient:

$n(k\nabla T) = -h_{loss}(T-T_{air})$ at x = -l/2 and x = l/2 (surface), ∀ y, z (5)

_The product bottom and the surfaces along the large waveguide walls are assumed to be thermally insulated.

$n(k\nabla T) = 0$ at z = - d, ∀ x, y (6)

$n(k\nabla T) = 0$ at y = -L/2 ∀x,z (7)

$n(k\nabla T) = 0$ at y = L/2 ∀x,z (8)

_The incident microwaves are generated on the inlet port in fundamental single-mode TE_{10}.

_The microwave power is absorbed without reflection at the waveguide outlet.

_The waveguide walls are assumed to be perfect electric conductors. There is therefore no electromagnetic power loss at the waveguide walls.

$n \times E = 0$ at x = -a/2 and x = a/2, ∀ y, z (9)

$n \times E = 0$ at y = -b/2 and y = b/2, ∀ x, z (10)

3.2. Simulation settings

The simulations were performed with the finite element software COMSOL Multiphysics, on a workstation with 256 GB RAM and an Intel® Xeon® CPU E5-2680 v3 processor, 12 cores, 2.50 GHz. The mesh of the entire geometry, on which the electromagnetism is solved, is composed of 17672 tetrahedra measuring no more than 6.88 mm. The heat equation is solved in a sub-geometry with a more refined mesh of 1318 tetrahedra, measuring no more than 1.00 mm. When solving both the electromagnetism and the heat equation, a previous study showed that mesh independency is obtained for a maximum element size of 1.75 mm (Sadot et al., 2017).

3.3. Input parameters for the model

The model required product properties (physical, thermal and electrical ones) and process parameters like convective coefficient, nitrogen temperature and incident microwave power.

3.3.1. Physical and thermal properties

The dry matter of the product is measured by weighing gel samples before and after heating for 48 h in a stove at 104°C.The gel density was measured at 20°C in a helium pycnometer Accupyc 1330 (Micromeritics, France). The measurement takes about 10 min, which makes it impossible in frozen phase. Therefore, density in frozen phase is determined by a mixing model:

$$\rho_f = \left(\frac{x_i}{\rho_i} + \frac{x_{bw}}{\rho_w} + \frac{x_{dm}}{\rho_{dm}}\right)^{-1} \quad (11)$$

Methylcellulose powder density is also measured in the helium pycnometer.

The initial freezing temperature is a key parameter. During a slow freezing experiment in a domestic apparatus, the evolution of the temperature was measured with thermocouples. The gel was not a

pure product, so the beginning of the pseudo plateau is assumed to be the initial freezing temperature.

The thermal conductivity was obtained with the hot-wire probe method (Healy et al., 1976) at 5°C, -15°C, -20°C and -25°C with a raise of 5°C. Because of the phase change, the thermal conductivity was not measured at temperatures close to the initial freezing temperature because latent heat would have caused a measurement error. In fresh state the thermal conductivity is assumed constant and equal to the value measured at 5°C. The freezable water content and the heat capacity were determined by differential scanning calorimetry on a µDSC VII (TA Instrument, USA). Samples of 130 mg were introduced in a Hastelloy C alloy cell. The heat flux was measured for freezing from 20°C to -40°C and for thawing from -40°C to 20°C at a rate of 1°C.min^{-1} for two different samples. Because water is the only component assumed to solidify, the freezable water content was determined by calculating the ratio between the total enthalpy of the product and the latent heat of pure water.

3.3.2. Dielectric properties

The dielectric constant and dielectric loss factor were measured with an open-ended coaxial probe (Dielectric Probe Kit 85070^{E}, high temperature configuration, Agilent Technologies) connected to an electronic calibration module (85092-60010, Agilent Technologies). The probe was located in a freezing cabinet (range 150, FROILABO, France). A low power microwave at the desired frequency (2450 MHz) was emitted by a network analyser (E5062A, Agilent Technologies) to the surface of the product (cylinder of 60 mm height and 35 mm diameter). The reflected microwaves from the product surface were analysed by the network analyser that allowed determining the dielectric properties using an algorithm. This method is well adapted to the food product dielectric properties measurement (Sheen & Woodhead, 1999) and was recently used with success (Llave et al., 2016). The measurements were performed at stabilised temperature between 20°C and -40°C.

3.3.3. Heat transfer coefficient

The lumped-capacitance method was used to measure the heat transfer coefficient between the nitrogen and the gel surface. An aluminium bloc with the same dimensions as those of the sample, with the same exposed surface and the same thermal insulation, was used. Aluminium was chosen because of its high thermal conductivity, which enables assuming a homogeneous temperature within this small volume. Assuming the perfect insulation of the aluminium bloc by the polystyrene on the surfaces not exposed to the nitrogen, the following equation can be written:

$$mCp\frac{dT_{alu}}{dt} = hS\left(T_{N_2} - T_{alu}\right) \qquad (12)$$

The nitrogen gas temperature has to be as constant as possible. The nitrogen delivery pipe is cooled, and then connected to the applicator once the temperature is stable. The convection coefficient is obtained by plotting:

$$\frac{mC_p}{S} ln \frac{T_0 - T_{N_2}}{T_{alu} - T_{N_2}} = f(t) \quad (13)$$

The straight-line slope obtained provides the convection coefficient.

3.3.4. Incident microwave Power

A power measurement system is included in the microwave generator. Nevertheless, because of possible power losses (in connecters, coaxial cables, waveguide walls, etc.) between the emitter and the applicator, a power calibration was performed on microwave heating in simple conditions.

4. Results and discussion

4.1. Methylcellulose gel properties

4.1.1. Density

To validate the mixing model of density in the frozen phase, it was first used to calculate the methylcellulose gel density from water and methylcellulose powder densities in fresh state. The calculated density and the measured density at 18°C were 1040.5 $kg.m^{-3}$ and 1065 ± 15.47 $kg.m^{-3}$ respectively. The relative difference of 2.33% was low enough to allow the use of the mixing model in the frozen phase. The density of the frozen gel obtained from the methylcellulose powder and ice densities was 966 $kg.m^{-3}$. Although there was a little difference between the frozen and fresh gel densities, the volume variation during the process (7.5%) was neglected. The frozen and fresh gel densities were used only to solve the heat equation.

4.1.2. Dry matter content

The dry matter measured was 0.129$kg.kg^{-1}_{product}$ ± 0.001 $kg.kg^{-1}_{product}$, which is logical regarding the formulation of the gel (13% powder).

4.1.3. Initial freezing temperature

Because of its considerable hydration, the beginning of the methylcellulose gel freezing plateau was horizontal. The initial freezing temperature was determined graphically at -0.7°C from the plateau following the supercooling break.

4.1.4. Thermal conductivity

The methylcellulose gel thermal conductivities measured from the hot–wire probe method are shown in Table 1. The values are in the range of data measured by previous authors (Otero et al., 2006; Singh & Heldman, 2014).

4.1.5. Freezable and bound water content

The latent heats obtained by DSC for freezing and thawing are presented in Table 2.

$$x_{fw} = \frac{Hf_{gel}}{Hf_w} = \frac{253.23}{332} = 0.7627\ kg_w.kg_{product}^{-1} \quad (14)$$

$$x_{bw} = x_w - x_{fw} = 0.8709 - 0.7627 = 0.1082 kg_w.kg_{product}^{-1} \quad (15)$$

The freezable water content is 0.7627 $kg.kg^{-1}$ of product and the bound water content is 0.1082 $kg.kg^{-1}$ of product.

4.1.6. Heat capacity

The heat capacity measured in fresh (20°C) and frozen (-20°C) phase is shown in Table 3.

4.1.7. Dielectric properties

The dielectric properties are presented in Figure 3. To the best of our knowledge, the dielectric properties of methylcellulose gel with 87% water content had not yet been measured experimentally. Nevertheless, during thawing, the evolution of dielectric properties as a function of temperature was very similar to that of other studies although the order of magnitude changed slightly due to a difference in hydration level (Llave et al., 2016) or due to the addition of salt (Nelson & Datta, 2001). The temperature dependencies of ε' and ε'' were observed in fresh state, especially for the dielectric loss factor (60% from 40°C to 0°C). Once the temperature reached the initial freezing point, an abrupt decrease in dielectric properties could be seen. Then, as the temperature decreased, the dielectric properties tended to stabilise around -10°C. This decrease of the dielectric loss factor as a function of temperature is commonly observed for a methylcellulose gel in fresh state without any addition of salt (Llave et al., 2016). With the gel used in the current study, the dielectric loss factor was more than 100 times lower at -20°C (0.25) than at 0°C (29).

As dielectric properties do not change greatly in the frozen phase, they were therefore considered constant in the model. The evolution of dielectric properties in the frozen phase was thus a function of the mixing model which depended on the ice fraction (Sadot et al., 2017). However, as they vary too much in fresh state, their variation was taken into account.

4.2. Convection coefficient

The convection coefficients between nitrogen and the aluminium bloc measured experimentally are reported in Table 4 for different trials.

Large differences in convection coefficient values were found. The measurement was reproducible but the nitrogen flowrate varied. The experimental device was equipped with a safety valve, which opened to avoid overpressure and induced nitrogen flow variations. Because of these variations, the convection coefficient was used as a fitting parameter in the range of the values measured.

4.3. Calibration of incident microwave power

The incident power at the applicator inlet had to be calibrated because of possible losses between the microwave generator and the applicator. 3D numerical simulations were performed on specific experiments of microwave heating of samples at ambient temperature for 1 minute. As the incident power was the only unknown parameter, it was calibrated by fitting the experimental temperature data with a numerical prediction.

As expected, the power supplied by the generator was higher than the incident power at the applicator inlet used as a boundary condition in the simulations. The generator power had to be corrected by a factor equal to 0.75 to obtain the incident power at the applicator inlet. This value was in in the range of the typical efficiency factor, which varies between 0.5 and 0.9 (Cherbanski, 2011; Wang et al., 2015). In these conditions, the resulting simulated temperature curves are very close to the experimental ones (Figure 4). The slight difference observed, approximatively 1°C, can be attributed to the hypothesis made for the simulation (such as perfect thermal insulation), and to experimental uncertainties. The calibration factors obtained from these heating experiments were applied for all the further microwave assisted freezing experiments.

4.4. Development of the hybrid 2D-3D model

The computation time of microwave assisted freezing can be very long. As a 4 g sample can be frozen in less than an hour experimentally, the computation can last more than a week. Thus a hybrid model was developed to reduce the computation time. The resolution of the electric field induced a 3D simulation because the geometry used in this study did not allow any geometrical simplifications along the y-axis (Figure 2). However, the heat equation did not need to be solved in 3D because the heat transfer was assumed to be homogeneous along the y-axis (Figure 2). The heat equation was then solved in 3D for a thin layer of 1 mm along the y axis, as shown in Figure 2b. This simplification can be assimilated to a 2D resolution on the x-z plan at y = 0. The temperature and thus the

297 temperature dependant dielectric properties required to solve Maxwell's equations are considered
298 constant along the y axis.
299 The results of hybrid and 3D models were compared for the microwave heating trial used to calibrate
300 the incident power at the applicator inlet (Figure 5). As the temperature curves at 2 mm and 7 mm
301 depth are very similar, it allows concluding that the hybrid model is relevant with this geometry.
302 Moreover, in this simple case of microwave heating without phase change, the hybrid model was 19
303 times faster than the full 3D model (3 min 48 s vs 71 min).

304 ## 4.5. Model validation

305 The current model was assessed previously (Sadot et al., 2017) in comparison to cryogenic freezing
306 (Rouaud & Le-bail, 2015) and microwave heating (Curet, 2008) because previous experimental
307 studies did not provide any exploitable data of microwave assisted freezing. According to our
308 knowledge, the current study is the first to provide relevant data available for model validation. In
309 the current study, the results of the model are compared to experimental results in controlled
310 conditions for the same geometry as that used for the microwave heating (Figure 2).

311 The global thermal losses at the product lateral walls were found to be low. The global thermal loss
312 coefficient ranged between 4.5 $W.m^{-2}.K^{-1}$ and 5 $W.m^{-2}.K^{-1}$. For all the simulations, the empirical
313 parameter of crystal growth (Y in Eq 6) was set to 0.75 K and provided the following ice content in
314 the gel (Figure 6). The ice mass fraction is dependent on the freezing kinetics. The empirical
315 parameter could not be determined by DSC by adjusting the freezing rate because of the
316 supercooling phenomenon that occurs systematically during freezing in the DSC oven.

317 Validation was done first for continuous applied microwave assisted freezing at a power of 1 W. The
318 convection coefficient was set at 95 $W.m^{-2}.K^{-1}$ on the cooled surface (Figure 7a). The model was then
319 used for pulsed microwave assisted freezing for a duty ratio of 0.33 and a power of 3 W (Figure 7b),
320 as electromagnetic wave assisted freezing was mainly performed with pulses in the literature (Anese
321 et al., 2012; Hafezparast-moadab et al., 2018; Xanthakis et al., 2014). In this second case, the
322 convection coefficient was 87.5 $W.m^{-2}.K^{-1}$.

323 In both cases, there was very good agreement between the simulated and experimental temperature
324 curves, although the temperature at 2 mm depth was slightly underestimated by the model. For
325 pulsed microwave assisted freezing, the temperature oscillations were about 1°C at 7 mm depth in
326 both the simulation and the experiment. At 2 mm depth, the temperature oscillations were smaller
327 in the simulation due to small uncertainties. It is also noteworthy that the temperature oscillations
328 disappeared once the initial freezing was reached and thus when the dielectric properties started to
329 decrease. The good agreement between the simulations and the experiments validated the model,

thereby making it possible to obtain information on phenomena previously impossible to obtain experimentally, such as electric field and generated heat distribution.

4.6. Analysis of interactions between microwaves and matter

The numerical study of microwave assisted freezing was conducted on continuous applied microwave assisted freezing at a power of 1 W. The electric field and the generated heat are plotted on the x-z central product section (y = 0) at several times (Figure 8).

First, we note that, contrary to the study in which the entire section (86 × 43 mm) was filled to a height exceeding 30 mm (Sadot et al., 2017), the heterogeneity of the electric field distribution was narrower (on the top surface the relative difference between the centre and the edges was 25% vs 95% in fresh state whereas it was 1% vs 95% in frozen state). This means that the objective of this geometry, i.e. to obtain considerable homogeneity in treatment along x axis (Figure 2), was achieved.

Secondly, the product was smaller in height (z axis) than in the previous study (Sadot et al., 2017). Only one maximum electric field appears in both the fresh and frozen phases (Figure 8a, c). After 15 minutes of microwave assisted freezing, two extrema of local electric field were visible due to the two phases separated by the freezing front (Figure 8b). There was only one local maximum of generated heat (hot spot), whose location corresponded to the local maximum of electric field in the fresh state (Figure 8d, e, f). After 15 min of freezing, although the electric field distribution was heterogeneous, it was in the same order of magnitude in the two phases (Figure 8b, Figure 9). The generated heat distribution was much more heterogeneous. It was much lower in the frozen phase compared to the fresh phase (Figure 8e, Figure 10). The freezing front, defined as the location where the temperature is at the initial freezing point, marks a clear separation of heat generated due to the reduction in dielectric loss factor, which was more than 100 times lower in frozen state (0.25 at -20°C) than in fresh state (29 at 0°C). Once the phase change began, the generated heat became very low (Figure 10) due to the fast decrease in dielectric loss factor (Figure 3).

In the previous numerical study (Sadot et al., 2017), the heat generated was high in the frozen phase because of the high electric field value and of the dielectric loss factor value taken from the literature (1.5 (Basak & Ayappa, 1997)) which was 6 times higher than the value measured in the current study (0.25).

The interest of using the numerical simulation of microwave assisted freezing results in better understanding of the interactions between microwaves and products during freezing. The significance of product height regarding homogeneous microwave treatment was presented here as an example in comparison with our previous study. It will be important to design the sample dimensions to study the impact of microwaves during freezing on ice crystal size. However, it is still

363 complicated to determine certain model inputs such as incident microwave power at the applicator
364 inlet due to power losses.

365 5. Conclusion

366 A laboratory scale microwave assisted freezing process was designed to conduct experiments with
367 parameters and conditions that were controlled as much as possible. The thermophysical and
368 dielectric properties of the methylcellulose gel were accurately measured and the incident power
369 was determined by the inverse method. A numerical model, developed previously, was improved by
370 using a hybrid method to solve the heat equation in 2D and the Maxwell equations in 3D. The
371 significant reduction of computational time allowed the validation of the model in comparison to the
372 experimental data with this geometry.

373 The results showed that the ice mass fraction approach that we proposed is relevant for describing
374 all the evolutions of all the thermophysical and dielectric properties during phase change. The ice
375 mass fraction can also be used to define the enthalpy variation in the range of temperature studied.

376 The numerical simulations used to observe the evolution of the temperature within the product were
377 in very good agreement with the experiments. They pointed out temperature oscillations only in the
378 fresh state before the phase change, when microwaves were applied by pulses. We also observed
379 the electric field and heat distribution generated in a small sample. Only one hot spot was detected
380 in both the entire fresh and the entire frozen sample (Figure 8d, e, f, Figure 10). During freezing, one
381 maximum electric field was found in each phase, separated by the freezing front. In the frozen phase,
382 the heat generated was much lower than in the fresh phase because of the huge decrease in
383 dielectric loss factor during freezing.

384 The present study first confirmed that this new experimental device is relevant for conducting
385 microwave assisted freezing experiments in controlled conditions. It also emphasised the importance
386 of product dimensions, especially height and width, for the thermal homogeneity of the product
387 during this novel freezing process. The results from this numerical simulation are very useful for
388 determining the optimal dimension of a sample that could be used to analyse the impact of
389 microwave treatment on ice crystal size. This is the main objective of the companion paper that deals
390 with the size of ice crystals according to process parameters (Microwave assisted freezing Part 2:
391 impact of duty cycle and microwave energy on ice crystal size distribution).

Acknowledgements

This work received financial support from the French National Research Agency (ANR) in the framework of the FREEZEWAVE project (ERANET call "SUSFOOD", grant number ANR-14-SUSF-0001). M. SADOT's PhD work is co-funded by the FREEZEWAVE project and the Région Pays de la Loire. The authors would also like to thank C. Couëdel for his technical contribution.

Nomenclature

a	Long waveguide wall length	(m)
b	Small waveguide wall length	(m)
Cp	Heat capacity	($J.kg^{-1}.K^{-1}$)
d	Product height	(m)
E	Electric field	($V.m^{-1}$)
H	Specific enthalpy	($J.kg^{-1}$)
h	Convection coefficient	($W.m^{-2}.K^{-1}$)
k	Thermal conductivity	($W.m^{-1}.K^{-1}$)
L	Product length (y axis)	(m)
Ls	Water latent heat of solidification	($J.kg^{-1}$)
l	Product width (x axis)	(m)
m	Mass	(kg)
n	Normal vector	
Q	Generated heat	($W.m^{-3}$)
S	Surface (m^2)	
T	Temperature	(K)
t	Time	(s)
x	Mass fraction	($kg.kg_{product}^{-1}$)
Y	Empirical parameter of the model	(K)
ε_0	Vacuum permittivity	($F.m^{-1}$)
ε"	Relative dielectric loss factor	
ρ	Density	($kg.m^{-3}$)
ω	Pulsation	($rad.s^{-1}$)

Subscript

air	Air
alu	Aluminium
bw	Bound water
d	Defrosted/fresh
dm	Dry matter
f	Frozen
i	Ice
N2	Nitrogen
w	Liquid water

References

Anese, M., Manzocco, L., Panozzo, A., Beraldo, P., Foschia, M., & Nicoli, M. C. (2012). Effect of radiofrequency assisted freezing on meat microstructure and quality. *Food Research International*, *46*(1), 50–54. http://www.sciencedirect.com/science/article/pii/S0963996911006491

Basak, T., & Ayappa, K. G. (1997). Analysis of microwave thawing of slabs with effective heat capacity method. *AIChE Journal*, *43*(7), 1662–1674. https://doi.org/10.1002/aic.690430703

Bremer, P. J., & Ridley, S. C. (2004). Safety of Frozen Foods. In Y. H. Hui, P. Cornillon, I. Guerrero Legaretta, M. H. Lim, K. D. Murrell, & W.-K. Nip (Eds.), *Handbook of Frozen Foods* (Marcel Dek, pp. 595–618).

Cherbanski, R. (2011). Calculation of Critical Efficiency Factors of Microwave Energy Conversion into Heat. *Chemical Engineering & Technology*, *12*, 2083–2090. https://doi.org/10.1002/ceat.201100405

Chourot, J. M., Macchi, H., Fournaison, L., & Guilpart, J. (2003). Technical and economical model for the freezing cost comparison of immersion, cryomechanical and air blast freezing processes. *Energy Conversion and Management*, *44*(4), 559–571.

Curet, S. (2008). *Traitements micro-ondes et transferts de chaleur en milieu multiphasique*. Thèse de l'Université de Nantes.

Dalvi-Isfahan, M., Hamdami, N., Xanthakis, E., & Le-Bail, A. (2017). Review on the control of ice nucleation by ultrasound waves, electric and magnetic fields. *Journal of Food Engineering*, *195*, 222–234. https://doi.org/10.1016/j.jfoodeng.2016.10.001

Delgado, A. E., & Sun, D.-W. (2001). Heat and mass transfer models for predicting freezing processes – a review. *Journal of Food Engineering*, *47*(3), 157–174. http://www.sciencedirect.com/science/article/pii/S0260877400001126

Dempsey, P., & Bansal, P. (2012). The art of air blast freezing: Design and efficiency considerations. *Applied Thermal Engineering*, *41*, 71–83.

Devine, C. E., Bell, R. G., Lovatt, S., & Chrystall, B. B. (1996). Red Meat. In L. E. Jeremiah (Ed.), *Freezing effects on food quality* (Marcel Dek, pp. 51–83).

Hafezparast-moadab, N., Hamdami, N., Dalvi-isfahan, M., & Farahnaky, A. (2018). Effects of radiofrequency-assisted freezing on microstructure and quality of rainbow trout (Oncorhynchus

462 mykiss) fillet. *Innovative Food Science and Emerging Technologies*, *47*(May 2017), 81–87.
463 https://doi.org/10.1016/j.ifset.2017.12.012

464 Hallstrom, B. (1990). Mass transport of water in foods - A consideration of the engineering aspects.
465 *Journal of Food Engineering*, *12*(1), 45–52. https://doi.org/10.1016/0260-8774(90)90018-4

466 Hanyu, Y., Ichikawa, M., & Matsumoto, G. (1992). An Improved Cryofixation Method - Cryoquenching
467 Of Small Tissue Blocks During Microwave Irradiation. *Journal of Microscopy-Oxford*, *165*(Part 2),
468 255–271.

469 Healy, J. J., de Groot, J. J., & Kestin, J. (1976). The theory of the transient hot-wire method for
470 measuring thermal conductivity. *Physica*, *82*(2), 392–408.

471 Jackson, T. H., Ungan, A., Critser, J. K., & Gao, D. (1997). Novel microwave technology for
472 cryopreservation of biomaterials by suppression of apparent ice formation. *Cryobiology*, *34*(4),
473 363–372. http://www.sciencedirect.com/science/article/pii/S0011224097920162

474 Jha, P. K., Sadot, M., Vino, S. A., Rouaud, O., Havet, M., Le-bail, A., Jury, V., & Curet-ploquin, S. (2017).
475 A review on effect of DC voltage on crystallization process in food systems. *Innovative Food*
476 *Science and Emerging Technologies*, *42*(May), 204–219.
477 https://doi.org/10.1016/j.ifset.2017.06.002

478 Kalichevsky, M. T., Knorr, D., & Lillford, P. J. (1995). Potential food applications of high-pressure
479 effects on ice-water transitions. *Trends in Food Science and Technology*, *6*(8), 253–259.

480 Le Bail, A., Chevalier, D., Mussa, D. M., & Ghoul, M. (2002). High pressure freezing and thawing of
481 foods: a review. *International Journal of Refrigeration*, *25*, 504–513.

482 Lim, M. H., McFetridge, J. E., & Liesebach, J. (2004). Frozen Food Components and Chemical
483 Reactions. In Y. H. Hui, P. Cornillon, I. Guerrero Legaretta, M. H. Lim, K. D. Murrell, & W.-K. Nip
484 (Eds.), *Handbook of Frozen Foods* (Marcel Dek, pp. 67–81).

485 Llave, Y., Mori, K., Kambayashi, D., Fukuoka, M., & Sakai, N. (2016). Dielectric properties and model
486 food application of tylose water pastes during microwave thawing and heating. *Journal of Food*
487 *Engineering*, 1–11. http://dx.doi.org/10.1016/j.jfoodeng.2016.01.003

488 Nelson, S. O., & Datta, A. K. (2001). Dielectric properties of food materials and electric field
489 interactions. In A. K. Datta & R. C. Anantheswaran (Eds.), *Handbook of microwave technology*
490 *for food applications* (pp. 69–114).

491 Otero, L., Ousegui, A., Guignon, B., Le Bail, A., & Sanz, P. D. (2006). Evaluation of the thermophysical

properties of tylose gel under pressure in the phase change domain. *Food Hydrocolloids*, *20*(4), 449–460. https://doi.org/10.1016/j.foodhyd.2005.04.001

Pangrle, B. J., Ayappa, K. G., Sutanto, E., & Davis, H. T. (1992). Microwave Thawing of Lossy Dielectric Materials. *Chemical Engineering Communications*, *112*(February), 39–53. https://doi.org/10.1080/00986449208935991

Rouaud, O., & Le-bail, A. (2015). *Optimizing Combined Cryogenic and Conventional*.

Sadot, M., Curet, S., Rouaud, O., Le-Bail, A., & Havet, M. (2017). Numerical modelling of an innovative microwave assisted freezing process. *International Journal of Refrigeration*, *80*, 66–76. https://doi.org/10.1016/j.ijrefrig.2017.04.017

Sheen, N. I., & Woodhead, I. M. (1999). An Open-ended Coaxial Probe for Broad-band Permittivity Measurement of Agricultural Products. *Journal of Agricultural Engineering Research*, *74*, 193–202.

Singh, R. P., & Heldman, D. (2014). Food Freezing. *Introduction of Food Engineering*, 540. https://doi.org/10.1016/B978-0-12-398530-9.00007-3

Taoukis, P., Davis, E. A., Davis, H. T., Gordon, J., & Talmon, Y. (1987). Mathematical Modeling of Microwave Thawing Modified Isotherm Migration Method. *Journal of Food Science*, *52*(2).

Wang, W., Zhao, C., Sun, J., Wang, X., Zhao, X., Mao, Y., Li, X., & Song, Z. (2015). Quantitative measurement of energy utilization ef fi ciency and study of in fl uence factors in typical microwave heating process. *Energy*, *87*, 678–685. https://doi.org/10.1016/j.energy.2015.05.036

Woo, M., & Mujumdar, A. (2010). Effects of Electric and Magnetic Field on Freezing and Possible Relevance in Freeze Drying. *Drying Technology*, *28*(4), 433–443. http://www.tandfonline.com/doi/abs/10.1080/07373930903202077

Xanthakis, E., Le-Bail, A., & Ramaswamy, H. (2014). Development of an innovative microwave assisted food freezing process. *Innovative Food Science and Emerging Technologies*, *26*, 176–181. http://dx.doi.org/10.1016/j.ifset.2014.04.003

Zhang, H., & Datta, A. K. (2005). Heating concentrations of microwaves in spherical and cylindrical foods. Part two: in a cavity. *IChemE*, *83*(March), 14–24. https://doi.org/10.1205/fbp.04047

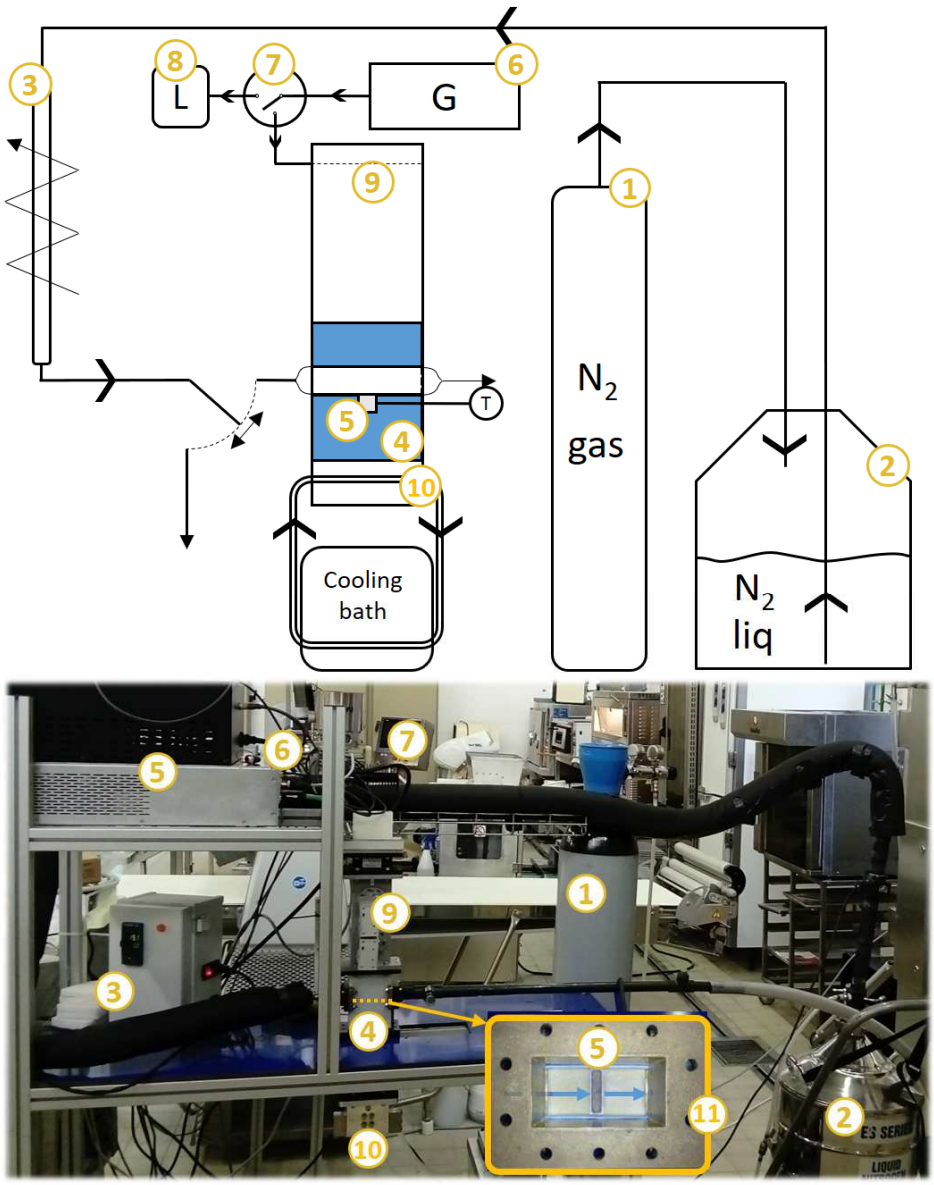

Figure 1: Scheme and photography of the experimental device of microwave assisted freezing process.

a)

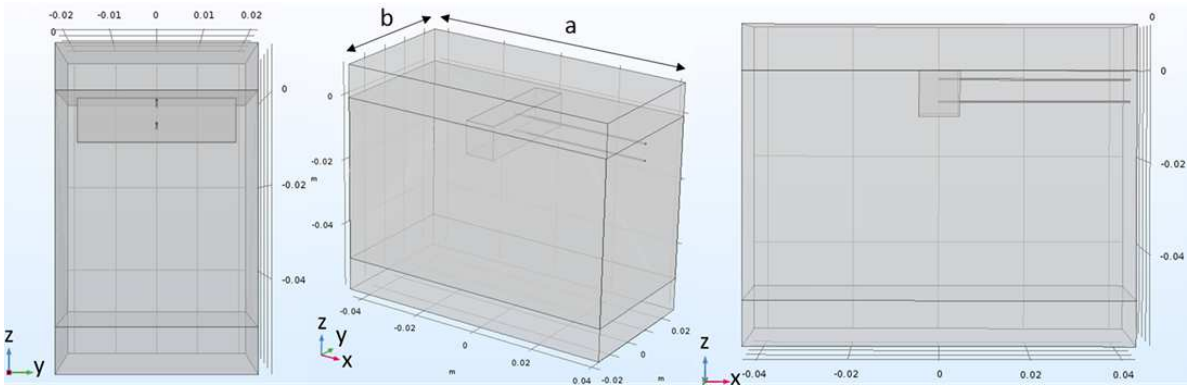

b)

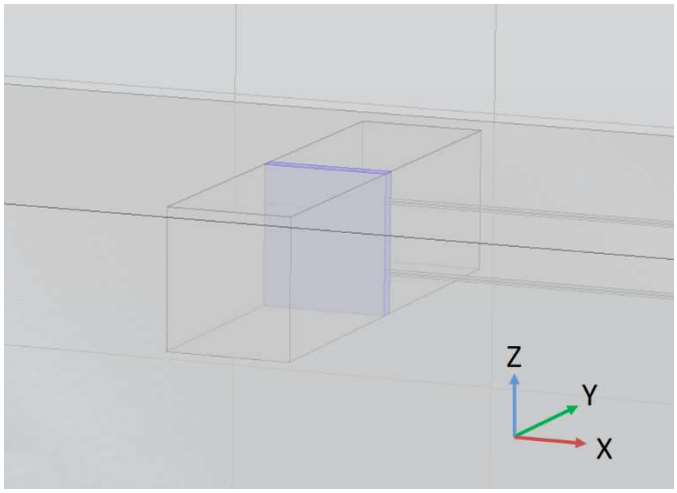

Figure 2: a) Geometry used to perform microwave assisted freezing trials and simulations, with thermocouples locations; b) layer on which the heat equation was solved for the hybrid model.

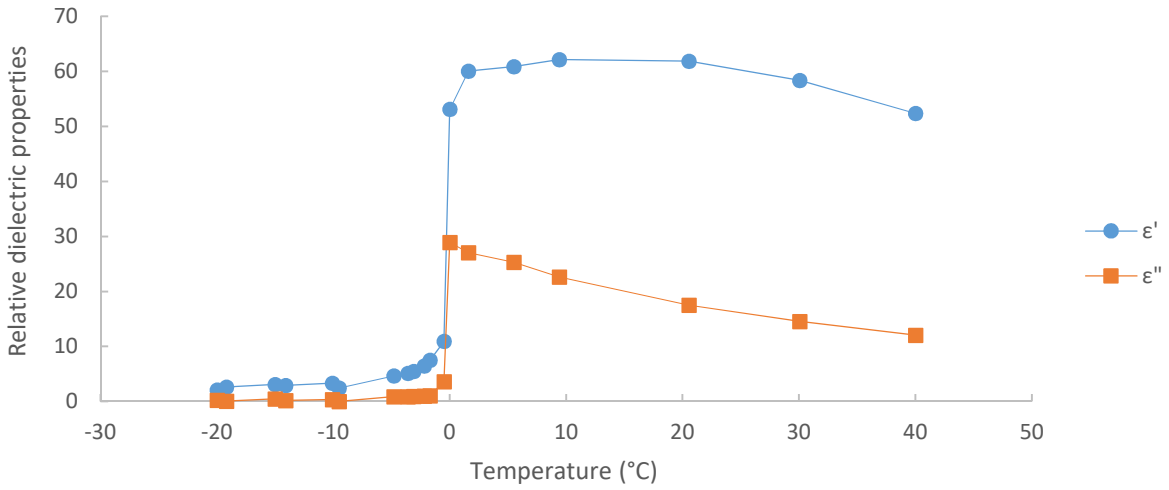

Figure 3: Dielectric constant (ε') and dielectric loss factor (ε") as a function of temperature.

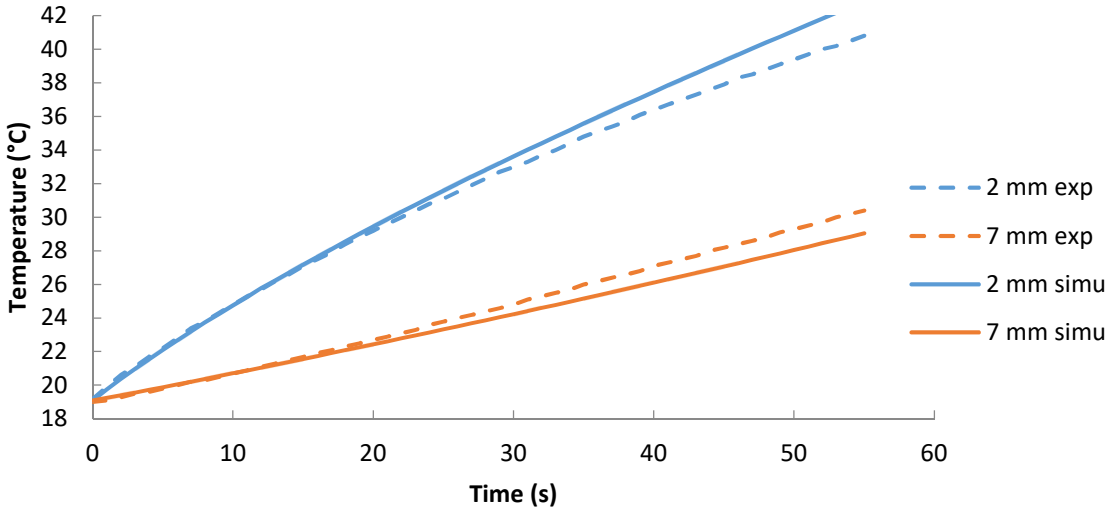

Figure 4: Comparison between experimental and simulated temperatures at 2 mm and 7 mm deep for a microwave heating at a measured power of 10.9 W (generator) with a resulting power of 8.2 W after using the calibration factor.

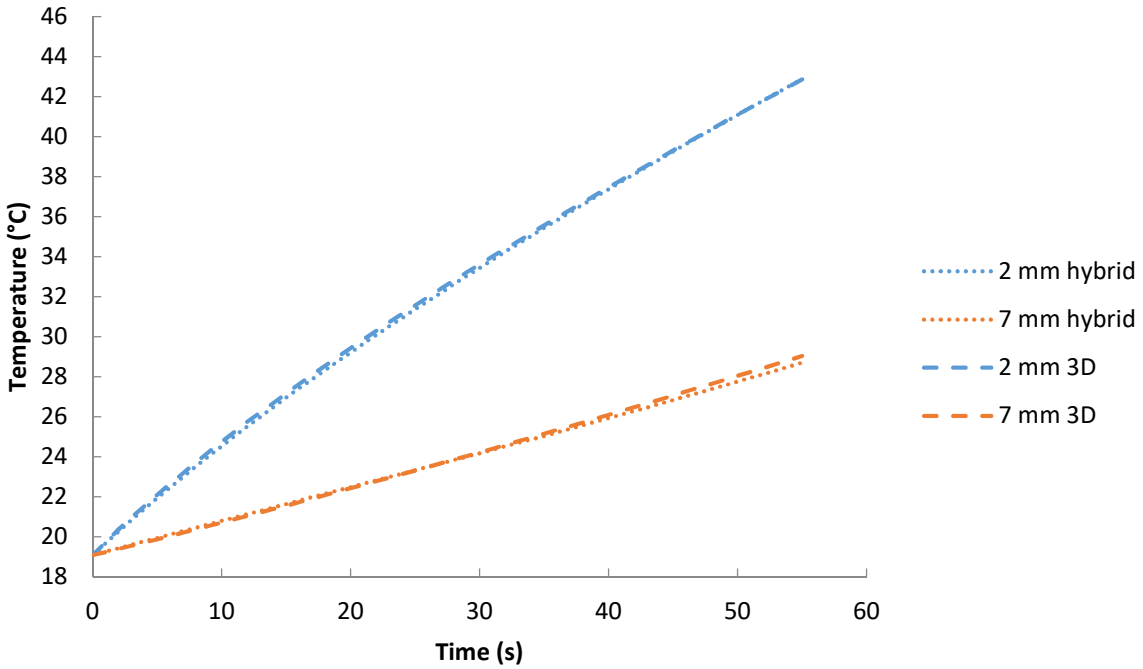

Figure 5: Comparison between hybrid and 3D model for a microwave heating.

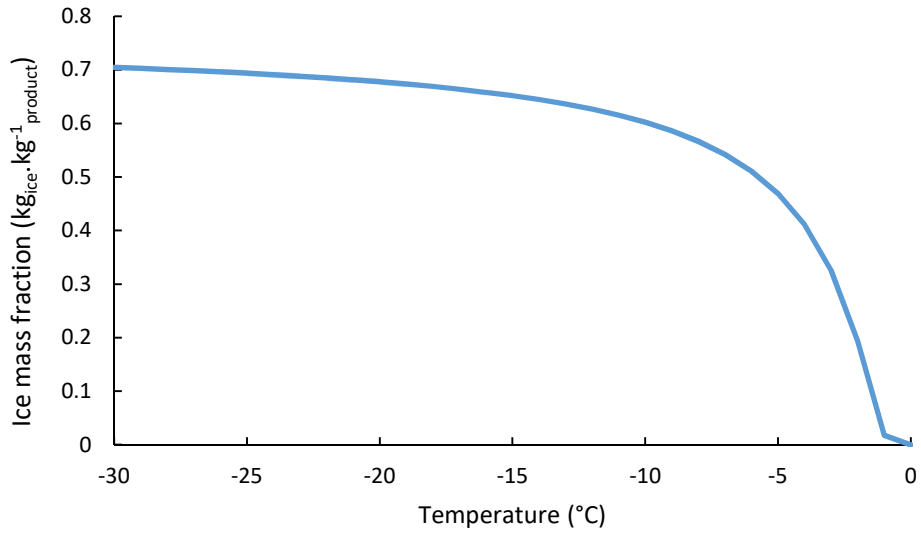

Figure 6: Ice mass fraction as a function of temperature for an empirical parameter Y set to 0.75 K

a)

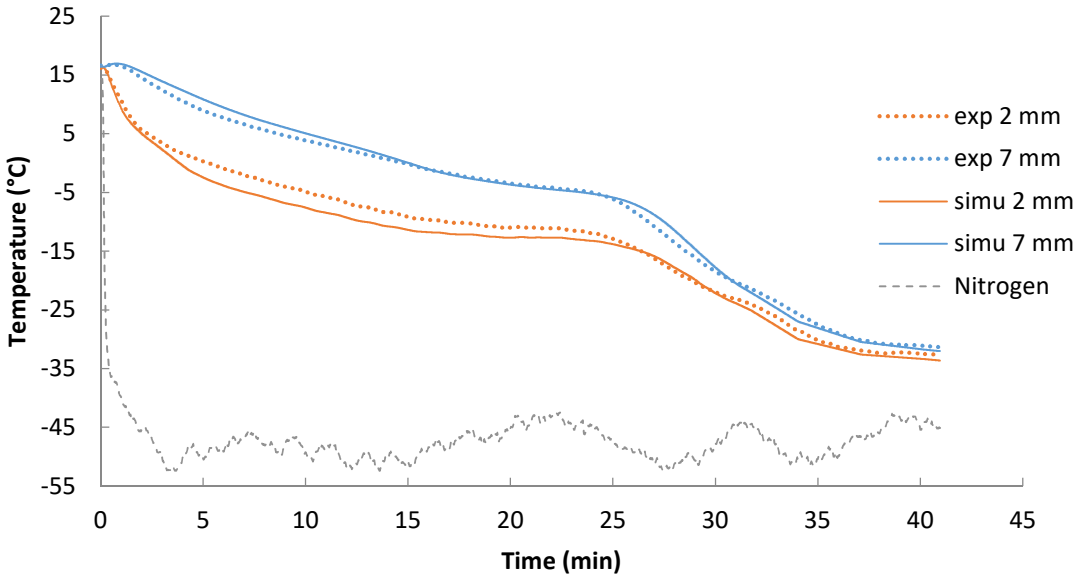

b)

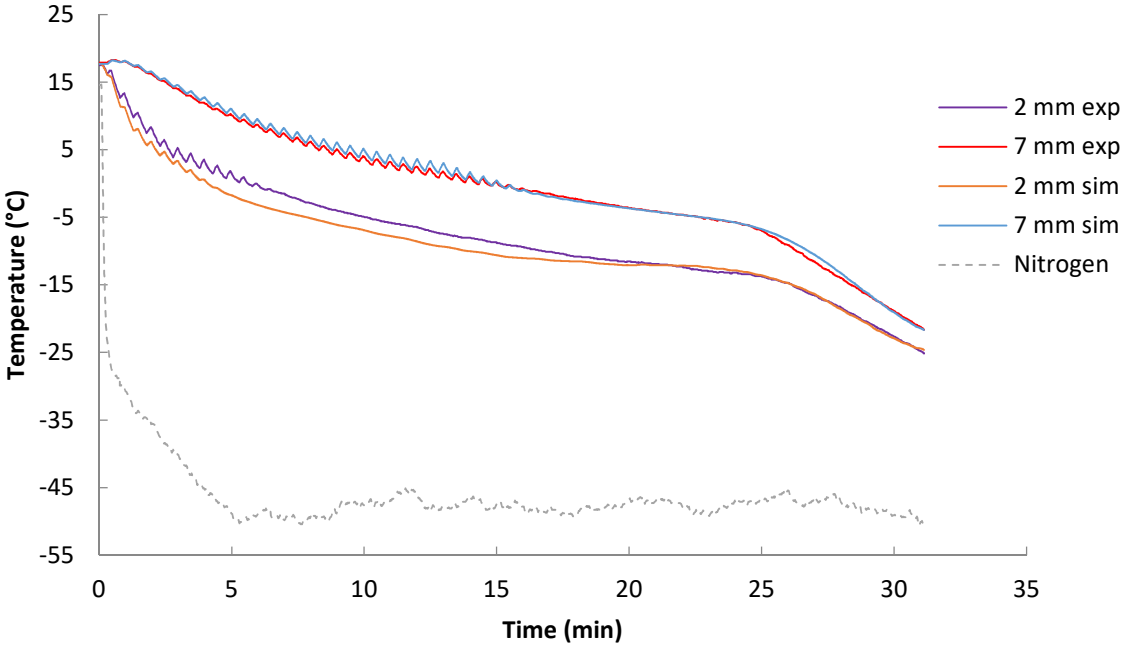

Figure 7: Comparison of temperature curves of a microwave assisted freezing a) for continuous application at a power of 1W; b) for a duty ratio of 0.33, a period of 30 s, at a power of 3 W.

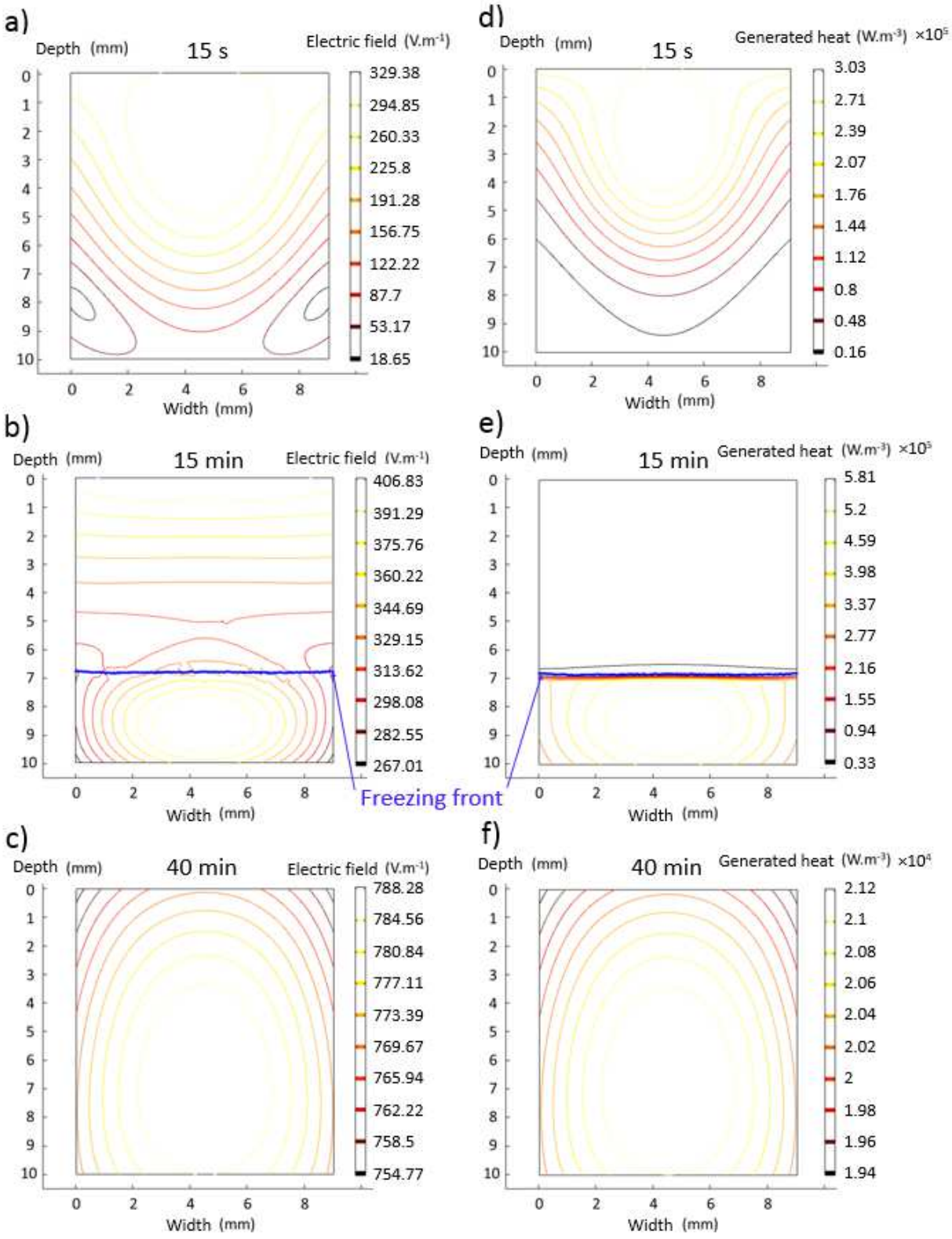

Figure 8: Electric field distribution in a) fresh state; b) during freezing; c) in frozen state; and generated heat in d) fresh state; e) during freezing; f) frozen state, on the x-z product central section (y = 0).

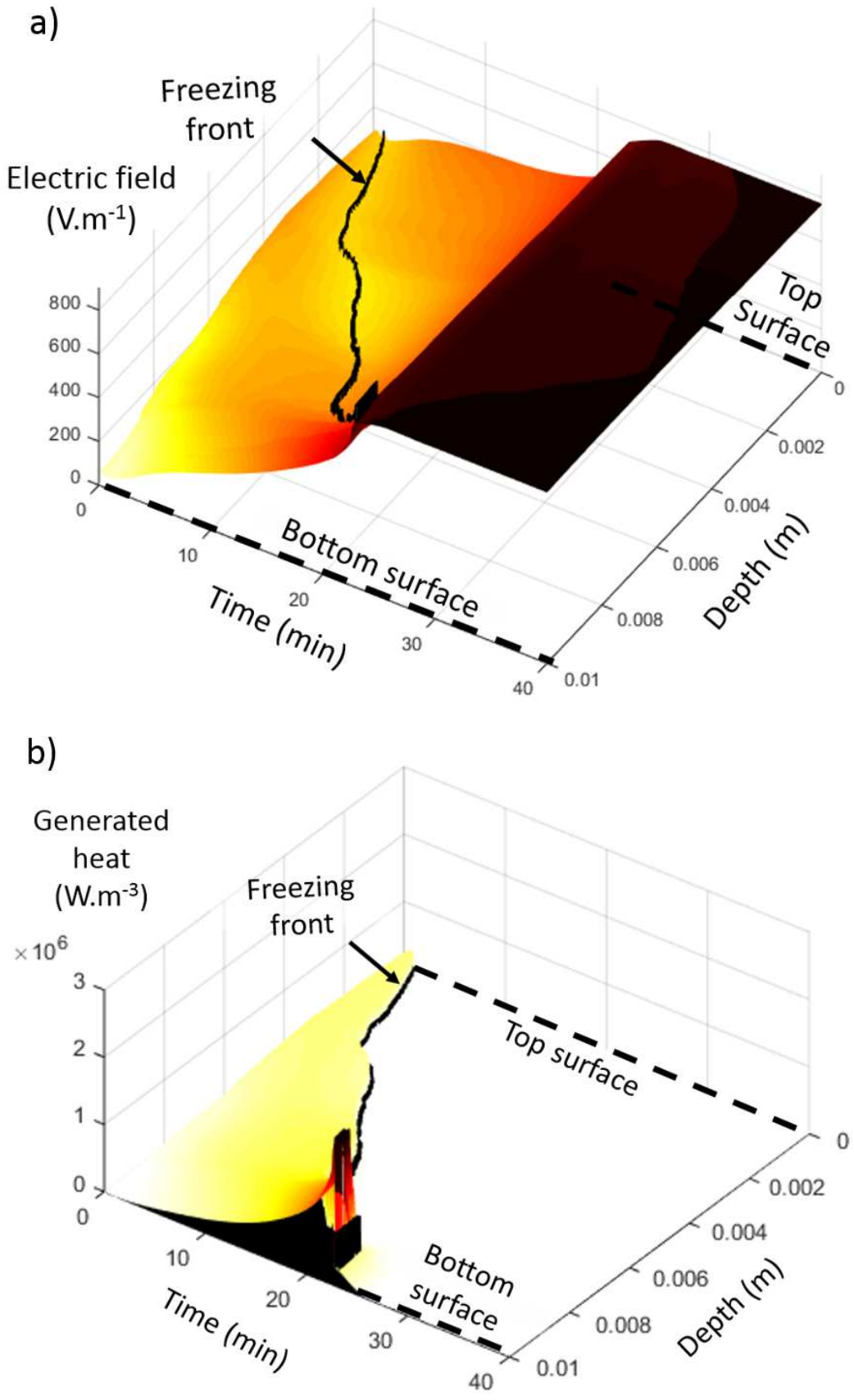

Figure 9: a) Electric field distribution; b) Generated heat distribution on the product z central axis (x = 0; y = 0) as a function of time and depth.

Table 1: Methylcellulose gel thermal conductivity at several temperatures, measured by hot-wire probe method.

Temperature (°C)	-25	-20	-15	5
Thermal conductivity ($W.m^{-1}.K^{-1}$)	1.670 ± 0.031	1.595 ± 0.279	1.556 ± 0.035	0.533 ± 0.018

Table 2: Latent heats measured by DSC during freezing and thawing of methylcellulose gel.

	Peak integration ($kJ.kg^{-1}$)	
	Freezing	**Thawing**
Trial 1	250.54	254.05
Trial 2	251.74	256.59
Mean latent heat ($kJ.kg^{-1}$)	253.23	

Table 3: Methylcellulose gel heat capacity in fresh and frozen phase.

		Trial 1	Trial 2	Mean
Heat capacity	**Fresh (20°C)**	3924.20	3881.18	3902.69
($J.kg^{-1}.K^{-1}$)	**Frozen (-20°C)**	2626.44	2587.8	2606.91

Table 4: Convection coefficient between nitrogen and aluminium bloc.

	Trial 1	Trial 2	Trial 3	Trial 4	Trial 5	Trial 6	Trial 7	Mean	Standard deviation
Convection coefficient ($W.m^{-2}.K^{-1}$)	124.5	118.0	125.1	86.2	123.5	104.2	109.5	113.0	14.3